Magnetic island-like patterns in synchrotron radiation images of JET runaway electron beams: a comparison between the JOREK simulation and experiments via synthetic camera diagnostics.

C. Sommariva[1], M. Hoppe[1], A. Pau[1], E. Nardon[2], G.T.A Huijsmans[2,3], M. Hoelzl[4], S.J.P. Pamela[5], V. Bandaru[6], C. Reux[2], O. Ficker[7], S. Silburn[8], J. Decker[1], J.P. Graves[1], JET Contributors[8,§], JOREK team[ᵛ], TSVV8 team and TSVV9 team

[1] *Ecole Polytechnique Fédérale de Lausanne (EPFL), Swiss Plasma Center (SPC), CH-1015 Lausanne, Switzerland*

[2] *CEA, IRFM, F-12108, Saint Paul-lez-Durance, France*

[3] *Eindhoven University of Technology, PO Box 513, 5600 MB Eindhoven, Netherlands*

[4] *Max Planck Institute for Plasma Physics, Boltzmannstr. 2, 85748 Garching bei München, Germany*

[5] *CCFE, Culham Science Centre, OX14 3DB, United Kingdom of Great Britain and Northern Ireland*

[6] *Indian Institute of Technology (IIT), Guwahati, Assam, India*

[7] *Institute of Plasma Physics of the CAS, CZ-18200, Praha 8, Czechia*

[8] *Eurofusion Consortium, JET Culham Science Center, Abingdon, OX14 3DB, United Kingdom*

[§] *See the author list of 'Overview of JET results for optimising ITER operation' by J. Mailloux* et al *2022* Nucl. Fusion *62 042026*

[ᵛ] *See the author list of 'M. Hoelzl, G.T.A. Huijsmans, S.J.P.Pamela, M. Bécoulet, E. Nardon, F.J. Artola, B. Nkonga et al., Nucl. Fusion 61 065001 (2021)'*

Plasma disruptions are global magnetohydrodynamics (MHD) instabilities leading to the termination of a tokamak plasma discharge [1]. Plasma disruptions are composed of a sudden loss of the plasma thermal energy, called thermal quench phase, followed by a decay of the plasma current up to discharge termination, called current quench phase [1]. After the current quench, a third phase, called runaway electron (RE) phase, may be observed [2]. The RE phase is characterised by the presence of a high current relativistic electron beam called RE beam. An uncontrolled strike of a RE beam on the reactor first wall can result in considerable damages such as: localised melting of the plasma facing components, coolant leakages and quench of superconducting coils [3]. Safe RE termination via disruptive MHD instabilities has been achieved by 1) compressing a beam until $q_a<2$ (TCV, ASDEX, DIII-D) or 2) massive deuterium injection (JET) [4]. Videos of the synchrotron radiation [5] emitted by RE beams of the JET tokamak in the IR and visible spectra [6] show the possible presence of island-like structures preceding RE benign termination [7]. The island structures is composed of two chains having poloidal mode number (m) of 4. RE benign termination can occur after the growth phase of the innermost m=4 chain [7]. Simulations performed using the JOREK code support the explosive growth and the overlap of two chains of m=4 magnetic islands as possible mechanism governing RE benign termination in JET experiments [8]. Despite the consistency between simulations and synchrotron images, further experimental evidence suggesting the presence of magnetic islands in JET RE beams has not been identified yet. For bridging the gap between JOREK RE simulations and JET experiments, a new synthetic camera diagnostic capable of rendering synchrotron images from kinetic (particle) simulations has been implemented in the JOREK code. The main objective is to reproduce synchrotron images of RE beams evolving in 3D MHD fields e.g, RE beams with double magnetic island chains. Two synchrotron radiation models are available in the JOREK synthetic camera: the full angular-spectral distribution (FASD - compatible with Lorentz's markers) [9] and the gyroaverage angular-spectral distribution (GASD - more adapted to guiding center markers) [10]. The two models are reported below:

$$P_R^{FASD}(\lambda,\psi,\chi) = \frac{ce^2}{\sqrt{3}\epsilon_0\kappa\lambda^4\gamma^2}(1+\gamma^2\psi^2)^2\left\{\left[\frac{\gamma^2\psi^2}{1+\gamma^2\psi^2}-\frac{1}{2}(1+z^2)\right]K_{\frac{1}{3}}(\psi)\cos\left[\frac{3}{2}\xi\left(z+\frac{z^3}{3}\right)\right]+ K_{\frac{2}{3}}(\xi)\sin\left[\frac{3}{2}\xi(z+\frac{z^3}{3})\right]\right\}$$

$$P_R^{GASD}(\lambda,\xi,\mu) = \frac{9e^2\beta^2\gamma^{12}\omega_B^3}{256\pi^3\epsilon_0 c^2\gamma_\parallel^2}\left(\frac{1-\beta\cos\psi}{\beta\cos\psi}\right)^2(1-\cos\theta_P\cos\mu)\left[K_{\frac{2}{3}}^2(\xi)+\frac{\beta\cos\psi\sin^2\psi}{2(1-\beta\cos\psi)}K_{\frac{1}{2}}^2(\xi)\right]$$

Comprehensive descriptions of all the terms of the full and gyroaverage synchrotron distributions can be found in [9-10]. Conversely, it is important to notice that FASD can have negative values if the angular values ψ, χ do not belong to certain intervals [9]:

$$\{\psi,\chi\} \notin [-\chi_c,\chi_c]\bigcap[-\psi_c,\psi_c]\ ,\psi_c = \left(\frac{3\kappa\lambda}{4\pi}\right)^{\frac{1}{3}}\ ,\frac{\gamma^3}{3}\chi_c^3+\gamma\chi_c-\frac{\pi}{3\xi}=0$$

The JOREK synthetic camera is based on the virtual point light (VPL) numerical method [11-13]. The VPL algorithm discretises both light sources and camera lens in a set of virtual light and gather points. In the VPL framework reflections and refractions are computed either generating secondary light points (biased) [11] or via path tracing techniques (unbiased) [13]. In JOREK, reflections, refractions and occluding surfaces have not been implemented yet while the camera model is an ideal perspective pinhole camera. Similarly, synchrotron lights are associated to the numerical particles used for the kinetic simulations of RE. Only the direct light emitted by each particle towards the pinhole camera is used for the rendering. After having defined an image plane, the light intensity received by the uvth-pixel is given by:

$$I_{uv}=\sum_{i=1,j=1}^{N_L,N_G} M_{ij}G_{ij}D_{ij}\ ,M_{ij}=S_{ij}\hat{\boldsymbol{n}}_G\cdot\frac{\boldsymbol{r}_{ij}}{r_{ij}},G_{ij}=\frac{V_{ij}}{r_{ij}^2}\ ,D_{ij}=\int_{\lambda_1}^{\lambda_2}P_R^{FASD,GASD}\left(\boldsymbol{x}_{G_j},\boldsymbol{x}_{L_i},\lambda\right)d\lambda$$

where N_L is the total number of particles, N_G is the total number of gather points (1 for pinhole camera), S_{ij} is the characteristic function of the sensor ($S_{ij}=1$ for ideal pinhole cameras), $\hat{\boldsymbol{n}}_G$ is the lens main direction of sight, $\boldsymbol{r}_{ij}=\boldsymbol{x}_{L_i}-\boldsymbol{x}_{G_j}$ is the ray connecting the ith light to the jth gather point and V_{ij} is the visibility function which is 1 if the ith light is visible by the jth gather point, 0 otherwise. Lights having rays outside the synchrotron emission cone [10] are discarded in JOREK to improve code performance. The FASD and GASD models have been tested using a JOREK equilibrium with hollow current density-j_ϕ profile. Markers have been initialised proportionally to j_ϕ and uniformly in momentum space [13]. The resulting initial RE distribution is:

$$f(R,Z,\phi,p,\theta,\zeta)=\frac{-6j_{\phi_{JOREK}}(R,Z,\phi)}{q\mu_0Rm^3c^4\left[\left(\frac{p^2}{m^2c^2}+1\right)^{\frac{3}{2}}-3\sqrt{\frac{p^2}{m^2c^2}+1}\right]_{P_1}^{p_2}[\cos^2\theta_1-\cos^2\theta_2][\zeta_2-\zeta_1]}$$

Where $j_{\phi\ JOREK}$ is the toroidal current density in JOREK units, $\{R,Z,\phi,p,\theta,\zeta\}$ are respectively the major radius, vertical position, toroidal angle, momentum, pitch and gyro angle coordinates, q,m are the particle charge and mass while μ_0,c are the vacuum permeability and the speed of light. The momentum, pitch and gyro angles are sampled within the intervals: $20MeV\ \pm 10keV$, $[\pi-0.295,\pi]$ and $[0,2\pi]$. The rendered synchrotron images are reported in fig.1 for the FASD (left plot) and for the GASD (right plot) models. Fig.1 shows that the FASD model provides unphysical negative radiation intensity as allowed by the model. Explanations for the FASD model unphysical result are under investigations but, possibly, they are related to the lack of non-negativity constraint applied to emission in the JOREK implementation. Conversely, the GASD model provides images with positive defined radiation intensities and reproduces the hollow synchrotron spot expected by the hollow j_ϕ profile. The synchrotron image renderer (GASD) has been tested performing a convergence study using the norm-2 error integrated over all pixels and computing the standard deviation (STD) of the light intensity for each pixel as a function of the number of lights. As reported in fig.2 upper plot, the convergence rate of the global norm-2 error is of 0.47 which is in line with the expected theoretical value for Monte-Carlo integrators of 0.5. Similarly, the correctness of synthetic camera implementation is supported by the STD which decays with a rate of 0.981, as shown in fig.2 lower plot for a set of randomly selected pixels. After having proved the statistical convergence

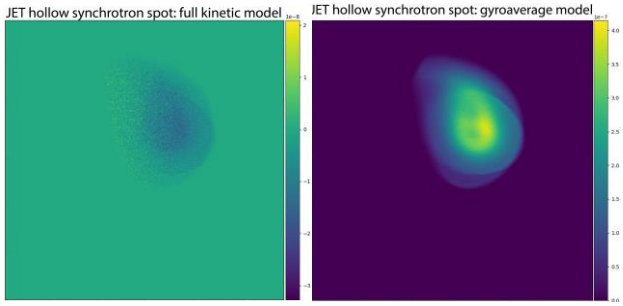

Figure 1 Synchrotron images of JOREK MHD equilibrium with hollow current profile using the FASD (left plot) and GASD (right plot) models

of the JOREK implementation, the bias error of the fast camera is estimated. The evaluation of the bias error is performed via direct comparison against images rendered by the SOFT code [10]. Even though that JOREK and SOFT render synchrotron images use the same GASD model, the two codes present markedly different implementations. Indeed, the SOFT numerical scheme is highly optimised for and limited to the rendering of synchrotron images from 2D magnetic field while the JOREK implementations allows the generation of RE beam images from arbitrary 3D time varying MHD fields. Consequently, an ad-hoc procedure is developed for benchmarking JOREK against SOFT. The first step consists of projecting the JOREK magnetic field onto the SOFT rectangular grid and of computing the radial RE distribution function needed by SOFT. The SOFT compatible distribution is obtained integrating the JOREK distribution along a flux surface and over the gyroangle. As second step, the SOFT simulation is run. The outputs generated by SOFT include the synthetic synchrotron image and the particle status at each orbital position. The particle position, momentum, and guiding center jacobian produced by SOFT are then used for generating a compatible marker distribution to be used in JOREK. The main manipulations needed for generating a JOREK compatible marker population is the increase of the number of particles randomizing their toroidal angle and the computation of the particle weights. The particle weights are given by $w_p = -2\pi f_{SOFT} J_{GC,SOFT} p^2 \Delta s \Delta t \Delta\phi \Delta p \Delta \cos\theta$ and represent the number of physical particles per numerical marker. Fig.3 upper left and upper right plots report the synthetic synchrotron images respectively produced by the JOREK and the SOFT codes while the lower left and lower right plots of fig.3 show the normalised differences and error between the JOREK and SOFT images defined as $I_\Delta = \frac{I_{uv_{JOREK}}}{\max_{uv} I_{uv_{JOREK}}} - \frac{I_{uv_{SOFT}}}{\max_{uv} I_{uv_{SOFT}}}$ and $I_{err} = |I_\Delta|$. As shown in fig.3 lower left and right plots, JOREK and SOFT images are in qualitative agreement with a normalised error below ~10% almost everywhere. Discrepancies up to 30% are observed below magnetic axis – high field side sector of the spot (bottom-right of the image). JOREK underestimates the radiation of the main synchrotron spot while overestimates the emission of the synchrotron halo. The peculiar shape of the region of discrepancy (almost a straight line) suggests an imperfect SOFT to JOREK particle transformation to be the main cause for the increased error. Investigations aiming to improve the JOREK-SOFT benchmark are on-going. As final check, the ability of the JOREK synthetic camera to produce images from 3D MHD fields has been tested. For doing so, synthetic synchrotron images from a JOREK hollow-j_ϕ MHD equilibrium and its evolution to a configuration with a double chain of

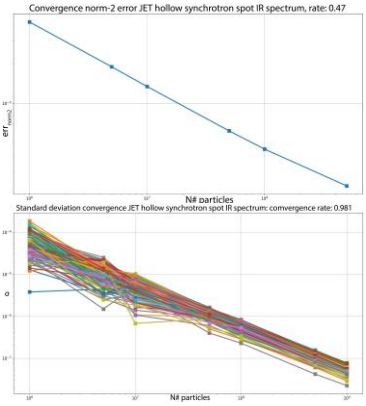

Figure 2 Norm-2 error convergence (upper plot) and per-pixel STD convergence (lower plot) studies with the number of lights

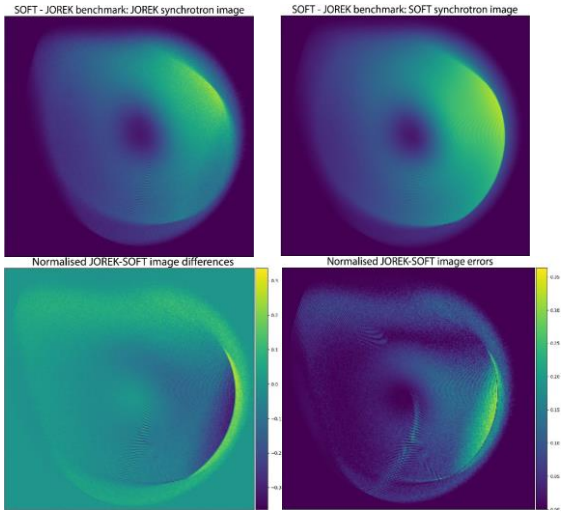

Figure 3 JOREK-SOFT benchmark: upper left and right plots are respectively the JOREK and SOFT RE images. Normalised JOREK-SOFT differences and errors are reported respectively in the lower left and right plots

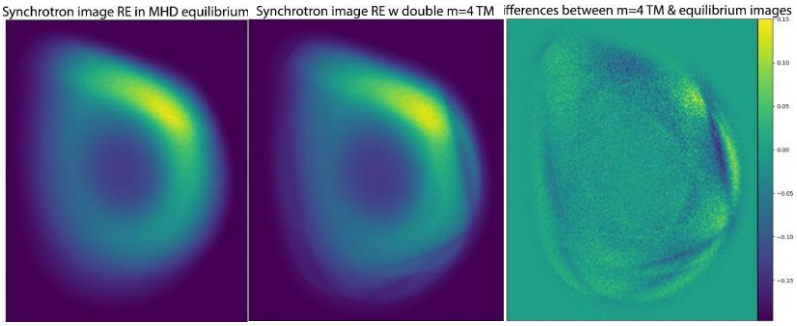

Figure 4 JOREK synthetic synchrotron images of an initial MHD equilibrium (left plot) and its evolution to a 3D configuration with double m=4 magnetic island chains (middle plot). The right plot is the difference between the equilibrium and the 3D MHD images.

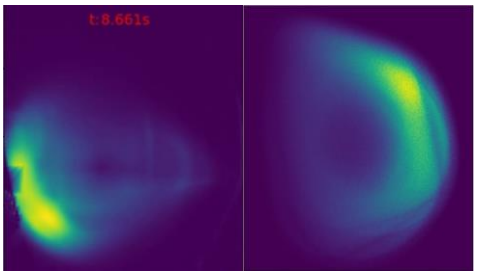

Figure 5 JET N# 95135 (left) and JOREK (right) IR images of RE beam with m=4 synchrotron islands. Note that the high field side is on the left for the experimental image and on the right for the JOREK image

m=4/n=1 (poloidal/toroidal mode numbers) magnetic islands [15] have been rendered. The resulting synthetic images are reported in fig.4 left plot for the MHD equilibrium and fig.4 middle plot for the double magnetic island chain cases. Similarly, fig.4 right plot shows the normalised differences between the 3D MHD and equilibrium images. Fig.4 middle and right plots reveal that both the inner and outer magnetic island chains are rendered as double chains of m=4 synchrotron islands visible in the synchrotron spot and in its halo region. 3D deformations of the j_ϕ distribution are correctly rendered as well. The test successfully proves the possibility of rendering synthetic synchrotron images from 3D MHD simulations using the JOREK synthetic camera. The generation of synthetic images from MHD simulations showing hollow-j_ϕ profiles and double magnetic island chains allows a preliminary comparison between JOREK RE calculations and the JET experimental data. Fig.5 presents a juxtaposition of the JET pulse 95135 IR image taken just before the RE benign termination (left plot) and the related double magnetic island chains simulated by JOREK (right plot). The main features observed in experiments are recovered by JOREK. Most notably, the hollowness of the synchrotron spot. Similarly, internal, and external synchrotron island chains can be identified in both the experimental and synthetic image (with a clear m=4 islands for the inner chain). However, substantial differences between the JET and the JOREK RE images are remain. Indeed, JOREK seems to overestimate the size of the synchrotron hollow region indicating that the initial MHD equilibrium used for JOREK simulations requires fine tuning. In addition, the external magnetic island chain appears to be a region of strong synchrotron emission (bright islands) in the JOREK image while in pulse 95135 the external islands are local minima of radiation (dark islands). A possible explanation to the discrepancy is that shaping of the RE momentum distribution is not considered in current simulations, where both energy and pitch angle are uniformly distributed. Finally, 3D deformations of the synchrotron spot predicted by JOREK are not visible in the pulse 95135 image. Therefore, the preliminary comparison between JOREK and JET RE beam synchrotron images suggests that full 5D-kinetic and 3D-MHD RE simulations with fine-tuned initial conditions are required for validating the RE benign termination mechanisms predicted by JOREK against JET experimental data. In conclusion, a 3D synthetic camera diagnostic has been implemented in the JOREK code. The JOREK camera has been used for rendering synthetic synchrotron images of RE beam using both FASD and GASD models. While the FASD model produced unphysical images, physically coherent images have been obtained using the GASD model and their convergence rate with the number of lights is successfully verified. The JOREK synchrotron camera implementation is in qualitative agreement with the SOFT code with a normalised error below 10% almost everywhere. A sector having error up to 30% has been found. The higher error is probably caused by discrepancies in the JOREK particle initialisation from SOFT data. First synthetic synchrotron images of 3D JOREK simulations presenting double chains of m=4/n=1 magnetic islands have been successfully rendered and a preliminary comparison against the JET pulse 95135 IR images has been performed. The comparison reveals that the main features observed in the experimental frame, such as synchrotron spot hollowness and synchrotron islands, are retrieved by JOREK. Conversely, improved MHD-kinetic simulations with fine-tuned initial conditions are required for validating the JOREK RE simulations against the JET experimental data.

This work has been carried out within the framework of the EUROfusion Consortium, via the Euratom Research and Training Programme (Grant Agreement No 101052200 — EUROfusion) and funded by the Swiss State Secretariat for Education, Research and Innovation (SERI). Views and opinions expressed are however those of the author(s) only and do not necessarily reflect those of the European Union, the European Commission, or SERI. Neither the European Union nor the European Commission nor SERI can be held responsible for them

[1] F.C. Schuller, Plasma Phys. Control. Fusion, vol.37, p.A135, 1995
[2] C. Reux et al., Nucl. Fusion, vol.55, p.093913, 2015
[3] G.F. Matthews et al., Phys. Scr., vol.T167, p.014070,2016
[4] C. Reux et al., Phys. Rev. Lett, vol.126, p.175001, 2021
[5] J. Schwinger, Phys. Rev., vol.75, 1912, 1949
[6] V. Huber et al., Nucl. Fusion, vol.58, p.076016, 2019
[7] C. Sommariva et al., Nucl. Fusion, 2023 (to be submitted to)
[8] V. Bandaru et al., Plasma Phys. Control Fusion, vol.63, p.035024, 2021
[9] L. Carbajal et al., Plasma Phys. Control Fusion, vol.59, p.124001, 2017
[10] M. Hoppe et al., Nucl. Fusion, vol.58, p.026032, 2018
[11] B. Walter et al., ACM Trans. Graph., 24, 3, 1081, 2005
[12] B. Walter et al. ACM Trans. Graph., 25, 3, 1098, 2005
[13] B. Walter et al, ACM Trans. Graph., 31, 4, 59 :1, 2012
[14] C. Sommariva et al., Nucl. Fusion, 2023 (to be submitted)
[15] E. Nardon et al., Phys. of Plasmas, 2023 (submitted)